JOURNAL OF BASIC SCIENCE AND ENGINEERING

DESIGN OF A UNIFIED CONVERTER FOR PMSM-BASED ELECTRIC VEHICLE DRIVE AND CHARGE FUNCTIONS

[1*]A. Kalyan, [2]S. Ravi Teja, [3]Pidikiti Tripura, [4]Kiran Kumar Malligunta

[1]PG Student, Department of Electrical and Electronics Engineering, Koneru Lakshmaiah Education Foundation, Guntur, AP, India. *Corresponding author E-Mail id: **kalyanananthulaelectrical006@gmail.com**

[2]Assistant Professor, Department of Electrical and Electronics Engineering, Koneru Lakshmaiah Education Foundation, Guntur, AP, India, Email id : **srungaramraviteja@kluniversity.in**

[3]Associate Professor, Department of Electrical and Electronics Engineering, RVR & JC College of Engineering, Guntur, AP, India, E-Mai id : **ptripura@rvrjc.ac.in**

[4]Associate Professor, Department of Electrical and Electronics Engineering, Koneru Lakshmaiah Education Foundation, Guntur, AP, India, E-Mai id : **mkkumar@kluniversity.in**

Abstract:

The present research describes an innovative approach to electric vehicle (EV) charging and driving integration that has been achieved through the construction of the Reconfigured Multi-Functional On-board Converter (RMOC). The RMOC system is a novel approach for unified charging and driving capabilities that uses a single-phase AC connection. The RMOC uses a novel DC-side switching network to rearrange existing electric vehicle drive components, removing the requirement for additional hardware generally required for charging and driving systems. This concept greatly reduces cost and size when compared to typical arrangements, making it a promising improvement in electric vehicle technology. Furthermore, RMOC connects effortlessly to normal single-phase power outlets, simplifying the charging process and lowering overall system complexity by eliminating the need for additional AC-side equipment like filters or relays. During charging, the RMOC achieves a unity power factor, guaranteeing that energy is efficiently transferred from the grid to the vehicle's battery. Importantly, the RMOC system is bidirectional, which allows for efficient power conversion in both charging and driving modes. To demonstrate its usefulness, it was tested successfully, showing seamless charging and driving modes. This study proposes a viable option for the future of electric car technology, with a streamlined and cost-effective strategy that makes the best use of existing on-board components.

Key Words: *The Power Converters, Battery, Ac and Dc Side switching network, electric vehicles (EVs), Bi-directional Converters, Reconfigured Multi-functional On-board Converter* (*RMOC).*

1. Introduction

The rise of electric vehicles (EVs) necessitates innovative solutions for onboard charging systems [1]. This paper explores the concept of Electric-Drive Reconstructed Onboard Converters (EDROCs), a technology that holds promise for streamlining and cost-effectively integrating charging and drive functionalities within a single unit [2-3]. EDROCs leverage existing electric vehicle drive components, eliminating the need for separate charging and drive systems. This approach offers significant size and cost reductions compared to traditional systems [4–5]. The core innovation lies in reconfiguring the DC side of the existing drive system using a switching network, enabling the system to seamlessly switch between charging and driving modes [6].

The EDROCs can be categorized based on the number of converters employed. Composite converter systems, often used in four-wheel-drive EVs or hybrid vehicles, are not suitable for single-motor EVs due to their complexity [7–8]. Double-stage converters, while applicable to most EVs, have more components compared to single-stage converters, making the latter a more cost-effective and compact solution for single-motor EVs[9–11]. One key challenge associated with EDROCs is their compatibility with conventional Permanent Magnet Synchronous Motors (PMSMs) commonly used in EVs[12–13]. PMSMs are not readily adaptable to reconfiguration for charging purposes [8–15]. Consequently, some research explores the use of specially designed motors with features like split windings or multiple winding sets. However, these designs often increase complexity compared to conventional PMSMs and introduce additional challenges, like insulation requirements.

This review highlights the potential of EDROCs for optimizing onboard EV systems. While challenges exist regarding motor compatibility, ongoing research in single-stage EDROCs using existing drive components presents a promising path for future development. A Novel Single-Phase Bidirectional Converter for Electric Vehicles: Leveraging Existing Hardware [16-20].

This paper presents a novel design for an electric vehicle (EV) onboard converter, the Electric-drive-reconstructed onboard converter (EDROC) [21–28]. Unlike previous approaches that relied on specially designed motors or additional bulky equipment, this EDROC utilizes the conventional Permanent Magnet Synchronous Motor (PMSM) commonly found in EVs. The key innovation lies in a switching network that reconfigures the DC-side of the existing drive system [29–30]. This eliminates the need for separate charging and drive systems, resulting in a simpler and more cost-effective solution. Additionally, the proposed converter eliminates the requirement for an external AC inductor, allowing it to directly connect to standard single-phase power outlets at home or work [31–33].

This paper introduces an innovative Single-Phase Bidirectional Electric-Drive-Reconstructed Onboard Converter (SBE-EDROC) designed specifically for electric vehicles (EVs). By leveraging a novel approach, the SBE-EDROC significantly enhances the efficiency and functionality of

onboard power conversion systems in EVs. Through a thorough analysis of the existing hardware infrastructure within EVs, this converter enables bidirectional power flow without requiring additional equipment, thus simplifying the integration process. Notably, the SBE-EDROC accommodates various traction hardware configurations, eliminating the need for motor-specific design constraints. Furthermore, its operation solely relies on single-phase power input, eliminating the necessity for auxiliary AC-side components like inductors or relays. Functionally, the SBE-EDROC seamlessly transitions between charging and driving modes, demonstrating robust performance characteristics in both scenarios. Simulation validation confirms the efficacy and reliability of the proposed SBE-EDROC, indicating its potential to revolutionize power conversion systems in the realm of electric mobility.

Traditional Electric-drive-reconstructed onboard converters (EDROCs) often require specially designed motors or additional bulky equipment like inductors or relays, increasing complexity and cost. These designs may not be compatible with conventional Permanent Magnet Synchronous Motors (PMSMs) commonly used in EVs. This research proposes a novel EDROC design that utilizes the conventional PMSM already present in most EVs. The design employs a switching network on the DC side of the existing drive system, eliminating the need for separate charging and driving systems. The proposed EDROC eliminates the requirement for an external AC inductor, allowing for direct connection to standard single-phase power outlets. This research makes a significant contribution to the field of EV technology. Simplifying and reducing the cost of onboard EV charging systems by leveraging existing hardware.

- Simplifying and reducing the cost of on-board EV charging systems by leveraging existing hardware.
- Promoting a more compact design by eliminating the need for additional inductors.
- Enhancing the integration of charging and driving functionalities within a single unit, leading to a more streamlined onboard system.
- Demonstrating the feasibility of using a single converter for both charging and driving modes with conventional PMSMs.

This novel EDROC design has the potential to significantly improve the efficiency and ease of use of onboard EV charging systems, paving the way for wider adoption of electric vehicles. This design offers several advantages. Firstly, it leverages existing drive components, minimizing additional hardware and associated costs. Secondly, the absence of a bulky AC inductor reduces the overall size and complexity of the system. Finally, the EDROC seamlessly integrates charging and driving functionalities within a single unit, promoting a more streamlined onboard system for EVs. The performance of the proposed EDROC is validated through both simulations and experimental results. This research paves the way for a future where EV charging becomes simpler and more efficient, leveraging existing hardware for a cost-effective and compact onboard solution.

Vol. 21, No. 1, (2024)
ISSN: 1005-0930

2. Analysis and Topology of the Reconfigured Multi-Functional On-board Converter (RMOC)

In this section, the **Reconfigured Multi-functional On-board Converter (RMOC).** that has been presented is broken down into its component parts in more depth. For the system configuration refer to figure 1 for a visual representation. The RMOC integrates seamlessly within a Plug-in Electric Vehicle (PEV) by connecting an auxiliary circuit between the battery and existing traction hardware (motor and inverter). This auxiliary circuit, along with the inverter, forms a switching network that reconfigures the system for charging or driving operation. A key advantage of this design is its compatibility. The proposed control method works with any traction hardware equipped with a three-phase inverter, eliminating the need for specially designed motors. Additionally, the converter simplifies the overall system design by using a single-phase power supply in place of additional AC-side components like relays or inductors. There are two different ways the RMOC can function: (A) charging mode and (B) driving mode.

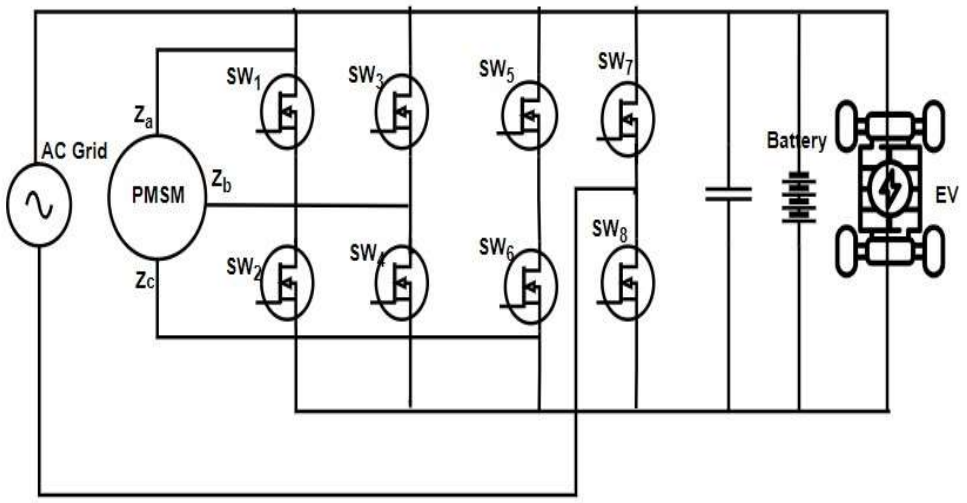

Figure 1. Reconfigured Multi-Functional On-board Converter topology.

A. Charging Mode

During charging, switches Sw_3-Sw_8 are turned on, while Sw_1 and Sw_2 remain off. The switching sequence is divided into eight states (refer to Figure 2 for details). These states depend on the polarity of the grid voltage.

$$Z_{S=}\begin{cases} Z_S \frac{di_{za}^I}{dt} = \frac{2V_{in}-V_B}{3} \\ Z_S \frac{di_{zb}^I}{dt} = \frac{2V_{in}-V_B}{3} \\ Z_S \frac{di_{zc}^I}{dt} = \frac{2V_{in}-V_B}{3} \end{cases}$$

(1)

where Vin is AC input voltages, V_B is battery voltages, and i_{za}^I', i_{zb}^I', and i_{zc}^I' are three-phase motor

Vol. 21, No. 1, (2024)
ISSN: 1005-0930

inductive currents in state I. Z_s inductance of the stator. Z_b stores energy in state I, and Z_c discharges it to the battery via switch SW_5. State II turns on switches SW_3, SW_6, and SW_8 and off switches SW_4, SW_5, and SW_7 (Figure 2(b)). State equation:

$$Z_s = \begin{cases} Z_s \frac{di_{Za}^{II}}{dt} = \frac{2V_{in}-V_B}{3} \\ Z_s \frac{di_{Zb}^{II}}{dt} = \frac{-V_{in}+2V_B}{3} \\ Z_s \frac{di_{Zc}^{II}}{dt} = \frac{-V_{in}-V_B}{3} \end{cases} \quad (2)$$

As can be seen in Figure 2(c), the switches SW_4, SW_6, and SW_8 are activated when the system is in state III, while the switches SW_3, SW_5, and SW_7 are deactivated throughout this condition. One way to express the state equation is as follows:

- ***Positive Grid Voltage (Switching State Mode I-IV)***

  Switch SW_7 is turned off in State I (figure 2(a)), whereas switch SW_8 is turned on. SW4 and SW_5 are conducting switches, whereas SW_3 and SW_6 are not conducting switches. It is through SW_8 that current is returned to the grid.

$$Z_s = \begin{cases} Z_s \frac{di_{Za}^{III}}{dt} = \frac{2V_{in}}{3} \\ Z_s \frac{di_{Zb}^{III}}{dt} = \frac{-V_{in}}{3} \\ Z_s \frac{di_{Zc}^{III}}{dt} = \frac{-V_{in}}{3} \end{cases} \quad (3)$$

$$Z_s = \begin{cases} Z_s \frac{di_{Za}^{V}}{dt} = \frac{2V_{in}-V_B}{3} \\ Z_s \frac{di_{Zb}^{V}}{dt} = \frac{-V_{in}+2V_B}{3} \\ Z_s \frac{di_{Zc}^{V}}{dt} = \frac{-V_{in}-V_B}{3} \end{cases} \quad (4)$$

State equations can be derived based on the system voltages and currents in each state. These equations consider factors like input AC voltage (V_{in}), battery voltage (V_B), and motor phase currents (iZ_a, iZ_b, iZ_c). During State I, inductor Z_b stores energy, and inductor Z_c discharges its stored energy to the battery through switch SW_5.

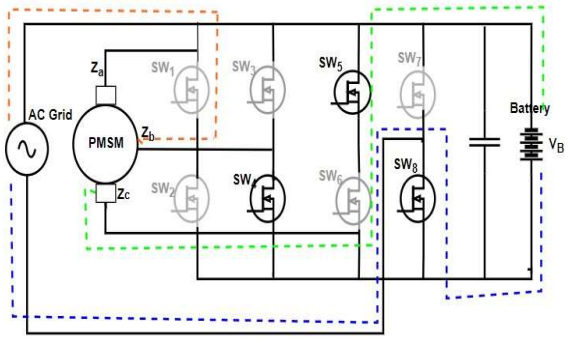

(a) Switching State Mode -I

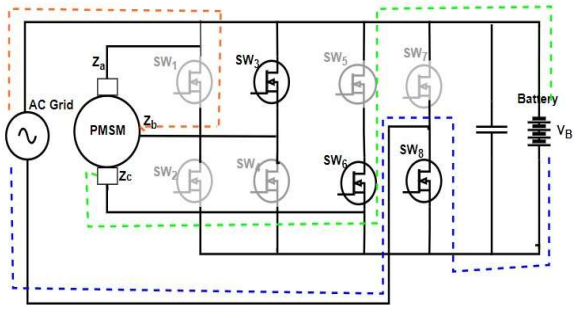

(b) Switching State Mode -II

Vol. 21, No. 1, (2024)
ISSN: 1005-0930

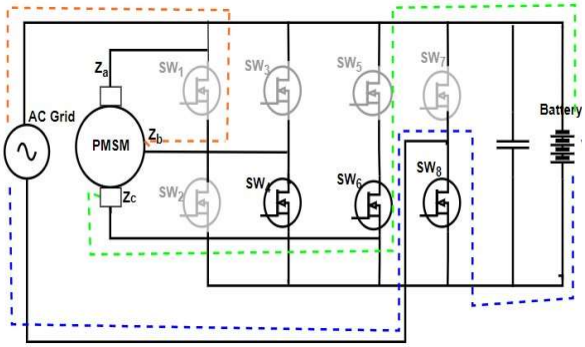

(c) Switching State Mode -III

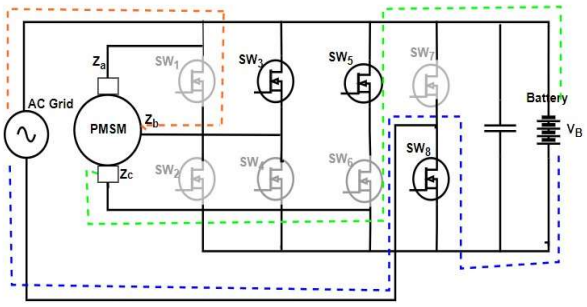

(d) Switching State Mode -IV

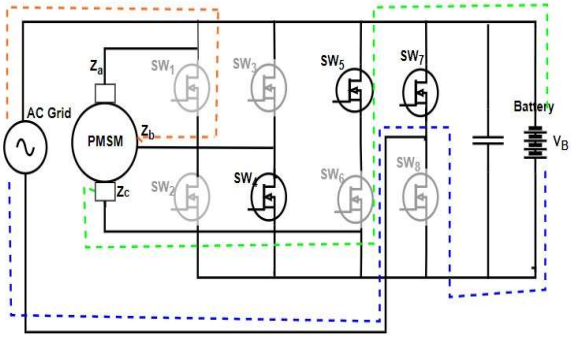

(e) Switching State Mode -V

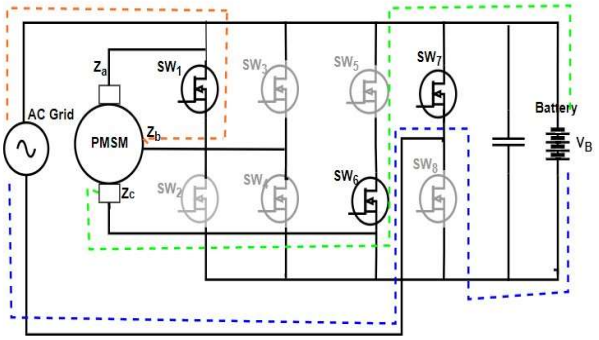

(f) Switching State Mode -VI

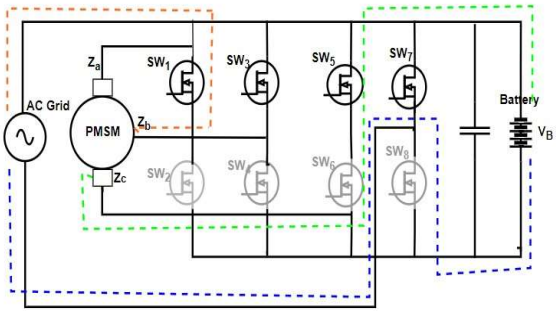

(g) Switching State Mode -VII

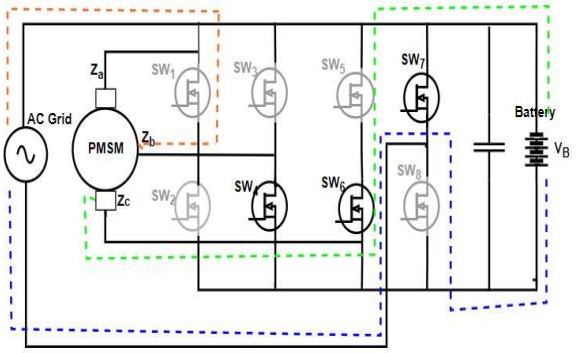

(h) Switching State Mode -VIII

Figure 2. Proposed RMOC charging mode state switching

- ***Negative Grid Voltage (Switching State Mode V-VIII)***

The switching pattern changes based on the negative grid voltage. The state equations can be similarly derived for each state, considering the reversed current flow.

$$Z_S = \begin{cases} Z_S \frac{di_{Za}^V}{dt} = \frac{-2V_{in}+V_B}{3} \\ Z_S \frac{diZ_b^V}{dt} = \frac{V_{in}+2V_B}{3} \\ Z_S \frac{di_{Zc}^V}{dt} = \frac{V_{in}-2V_B}{3} \end{cases} \quad (5)$$

$$Z_s = \begin{cases} Z_s \frac{di_{Za}^{W}}{dt} = \frac{-2V_{in}+V_B}{3} \\ Z_s \frac{di_{Zb}^{W}}{dt} = \frac{V_{in}-2V_B}{3} \\ Z_s \frac{di_{Zc}^{W}}{dt} = \frac{V_{in}+V_B}{3} \end{cases} \quad (6)$$

$$Z_s = \begin{cases} Z_s \frac{di_{Za}^{x}}{dt} = \frac{-2V_i}{3} \\ Z_s \frac{di_{Zb}^{x}}{dt} = \frac{V_m}{3} \\ Z_s \frac{di_{Zc}^{x}}{dt} = \frac{V_m}{3} \end{cases} \quad (7)$$

$$Z_s = \begin{cases} Z_s \frac{di_{Za}^{III}}{dt} = \frac{-2V_{in}+2V_B}{3} \\ Z_s \frac{di_{Zb}^{III}}{dt} = \frac{V_{in}-V_B}{3} \\ Z_s \frac{di_{Lc}^{III}}{dt} = \frac{V_{in}-V_B}{3} \end{cases} \quad (8)$$

According to the volt-second balance, the relationship between the input voltage and the output voltage can be obtained by using equation (1) through (8) as a starting point: Similar to State I, specific inductors store or discharge energy during these states.

Switching State Mode II-IV: Managing Energy Flow and Storage:

- ***Switching State Mode -II (Figure 2(b)):*** In this state, switch S3 is turned on, allowing inductor Lb to discharge its stored energy directly to the battery. Conversely, inductor Lc accumulates energy from the AC line voltage. The state equation reflects this energy transfer.
- ***Switching State Mode-III (Figure 2(c)):*** Here, switches S4, S6, and S8 are conducting. This configuration enables all three inductors (L_a, L_b, and L_c) to store energy directly from the AC line voltage. The corresponding state equation captures this energy storage process.
- ***Switching State Mode - IV (Figure 2(d)):*** This state involves the combined discharge of inductors Z_a, Z_b, and Z_c through switches SW_3 and SW_5. This discharged energy contributes to charging the battery. The state equation reflects this energy flow from the inductors to the battery.

The proposed converter exhibits two distinct operational modes within the positive grid voltage range, determined by the duty cycle (D) of switches Sw_4 and Sw_6:

$0 < D < 0.5$: When the duty cycle falls within this range, the switching sequence follows a specific pattern: Here is the sequence of states: ***Switching State Mode I → Switching State Mode - III → Switching State Mode II →Switching State Mode - III → Switching State Mode -I.*** This sequence ensures efficient energy management during charging.

$0.5 < D < 1$: As the duty cycle increases beyond 0.5, ***Switching State Mode - I → Switching State Mode - IV → Switching State Mode -II → Switching State Mode - IV → Switching State Mode -I*** is the next switching sequence that emerges after the previous one. This modified sequence reflects a different approach to energy flow within the system.

Interestingly, the operational behavior during negative grid voltage mirrors the operation observed

with positive voltage. The switching patterns and state equations adapt accordingly, considering the reversed current flow direction. By applying the principle of volt-second balance (considering the voltage across each element integrated over a switching period) and analyzing equations (1) to (8), we can establish a critical relationship between the input voltage (Vin) and the output voltage (VB) of the converter.

Identifying an equation where the inductor current is related to other variables, including the duty cycle and potentially some additional parameters. Next, expressing other variables in terms of the independent inputs using additional equations from the system. Substituting the obtained expressions into the equation from step 1 to eliminate unwanted variables. Finally, manipulating the resulting equation to isolate the inductor current on one side and the duty cycle on the other side. This process allows you to directly relate changes in the duty cycle to the resulting changes in the inductor current, providing a valuable tool for analyzing and controlling DC-DC converters.

This relationship can be expressed using the following equation:

$$\begin{cases} G = \frac{1}{1-D} \\ V_B = mV_mGsin(wt) \end{cases} \quad (9)$$

where G is the voltage gain; V_m is the amplitude of input voltage. m is the modulation index of the inverter.

V_m signifies the amplitude of the input AC voltage.

m denotes the modulation index of the inverter, a crucial parameter that influences the output voltage.

This equation highlights the dependence of the battery's charging voltage (VB) on the input AC voltage (Vin), the converter's voltage gain (G), and the inverter's modulation index (m). By manipulating these factors, the charging process can be effectively controlled. In essence, the RMOC's charging mode leverages a combination of switching states and duty cycle control to manage the flow and storage of energy within the inductors.

$$i_{C\_sw} = \frac{-V_{o\_sw}}{R}D + (i_{L\_sw} + \frac{-V_{o\_sw}}{R})D^1 = C\frac{dV_{o\_sw}}{dt} \quad (10a)$$

$$V_{L\_sw} = V_{s\_sw}D + (V_{s\_sw} - V_{o\_sw})D^1 = L\frac{di_{L\_sw}}{dt}$$

(10a)

The inductor average switching time voltage, V_{L_sw} in one switching cycle, and average inductor voltage as V_L and the average capacitor switching time current, i_{C_sw} in one switching cycle, and capacitor average current i_C are derived based on the equivalent circuit model as in Fig. 2 is shown in Eq. (10a) and Eq. (10b). Here, D' refers to off-time of the switching duty cycle (D) equal to (1-D). In the same way the output average voltage and input rectified source average voltage in one switching cycle is V_{o_sw} and V_{s_sw}.

We will now linearize Eq. (10a) and Eq. (10b) via perturbations, derived Eq. (11a) and (11b) are:

$$C(\frac{dV_o}{dt} + \frac{dv_o}{dt}) = \frac{-V_o}{R} + I_LD^1 + \frac{-v_o}{R} + i_LD^1 - i_Ld - I_Ld$$

(11a)

Vol. 21, No. 1, (2024)
ISSN: 1005-0930

$L(\frac{dI_L}{dt} + \frac{di_L}{dt}) = V_R - V_o D^1 + v_R - v_o D^1 + V_o d + v_o d$

(11b)

Where the perturbed voltages, v_R, v_o,and d are rectifier terminal voltage, output voltage, and duty cycle and the DC components parameters D' (which is 1-D), I_L, V_o, V_R off time duty cycle, inductor current, output terminal voltage, and rectifier terminal voltage. Equations (11a) and (11b) can be simplified by assuming zero direct current (DC) because the DC components on both sides of the equations are identical. Thus, equations (12a) and (12b) are derived.

$C\frac{dV_o}{dt} = \frac{-V_o}{R} + i_L(1-D) - I_L D$

(12a)

$L\frac{di_L}{dt} = v_R - v_o D^1 + V_o d$ (12b)

By employing substitution and isolating the independent inputs, the transfer function relating the duty cycle to the inductor current using the equations (12a) and (12b) can be obtained as in Equation (13). This technique involves expressing one variable in terms of another and then manipulating the equations to arrive at a relationship between the duty cycle and the inductor current.

$$G_{id} = \frac{i_L}{d} = \frac{V_o}{L} \frac{s + \frac{V_o + I_L R D^1}{V_o RC}}{s^2 + \frac{1}{RC}s + \frac{D^{12}}{LC}}$$

(13)

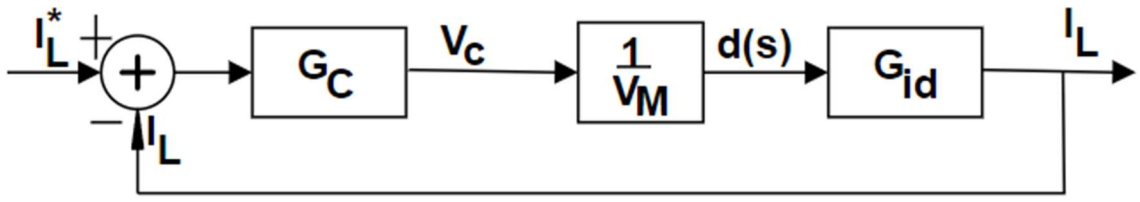

Fig.3 block diagram of the closed-loop current control loop.

The current controller's transfer function, denoted by GC, is presented in Equation (14).

$$G_C(s) = k\frac{1+sT}{sT}$$

(14)

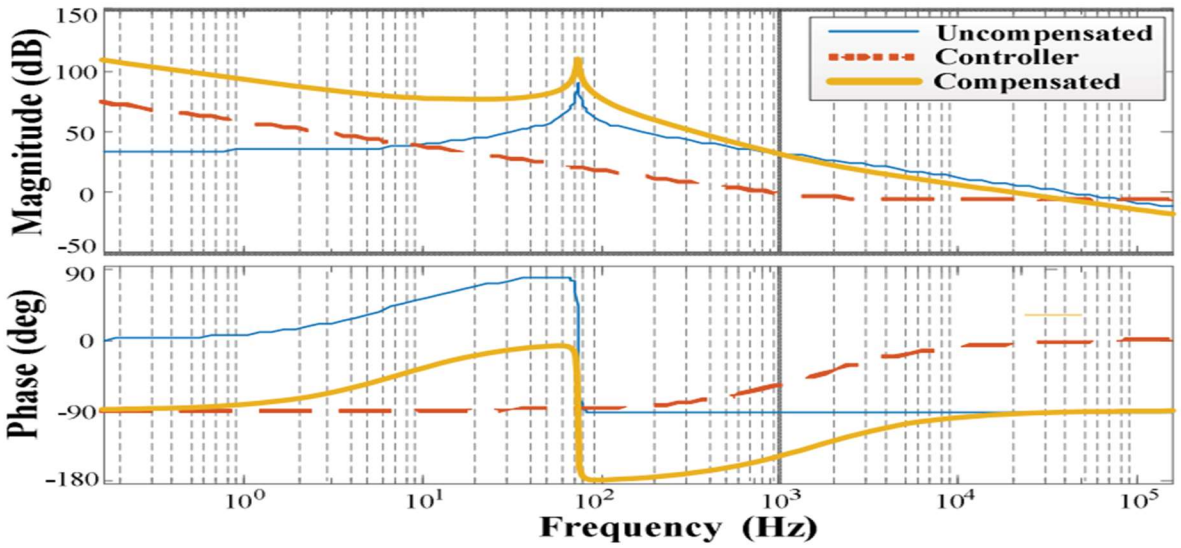

Fig. 4 Bode Plots of Uncompensated Loop, Current Controller, and Compensated Loop Transfer Functions

The system in Figure 5 can be characterized by its closed-loop transfer function, as given in Equation (15).

$$\frac{I_L}{I_L^*} = \frac{G_C G_{id}}{1+G_C G_{id}} \quad (15)$$

This strategic management ensures efficient energy transfer from the AC line to the battery, ultimately charging the electric vehicle's battery. This section provides a brief overview of the charging mode operation. Further details on the remaining states and their corresponding equations are likely presented in the full research paper. The charging circuit to analyze the system's stability is developed. The current controller is designed with a gain of 0.5 and a time constant of 100 µS. Figure 4 presents the Bode plots for three key transfer functions, such as, uncompensated loop transfer function, the compensated loop transfer function (which incorporates the controller), and the current controller transfer function itself.

The Bode plot analysis (Fig. 4) reveals a phase margin of 85.7° at the crossover frequency, indicating a stable system. As long as the compensator design (referring to the current controller) maintains a sufficient phase margin at low frequencies, the inner current loop should remain stable. With the inner current controller parameters chosen, we can now focus on designing the outer voltage loop, which controls the output voltage. Figure 4 depicts the block diagram of this outer voltage control loop.

B. Driving Mode: Powering the Electric Motor

The RMOC seamlessly transitions from charging to driving mode. Here's how it operates in this mode:

Switch Configuration: Switches Sw_1-Sw_6 are turned on, while Sw_7 and Sw_8 are disabled. This configuration essentially bypasses the auxiliary circuit, connecting the battery directly to the inverter.

Switching State Mode: The converter operates in eight distinct vector states, mimicking the operation

Vol. 21, No. 1, (2024)
ISSN: 1005-0930

of a traditional Sinusoidal Pulse Width Modulation (SVPWM) control method commonly used for Permanent Magnet Synchronous Motors (PMSMs) (refer to figure 4 and 5 for a visual representation). The proposed RMOC effectively controls the PMSM using the established SVPWM technique [23-25]. This method involves generating switching patterns for the inverter that create a desired voltage waveform, ultimately controlling the motor's speed and torque. The mathematical equations governing the motor's behavior in the driving mode are expressed in the d-q reference frame (a mathematical transformation that simplifies the analysis of AC motors). These equations capture the relationship between various electrical parameters and the resulting torque generated by the motor. State Equations (Equation 10).

$$\begin{cases} u_d = R_s i_d + P\psi_d - \omega_r \psi_q \\ u_q = R_s i_q + P\psi_q + \omega_r \psi_d \\ T_e = P\left(\psi_d i_q - \psi_q i_d\right) \end{cases} \quad (10)$$

Where: Rs: Stator resistance of the motor

id, iq: d-axis and q-axis stator currents, respectively

ψd, ψq: Permanent magnet flux linkage in the d-axis and q-axis, respectively

ωr: Rotor speed

Te: Electromagnetic torque produced by the motor

These equations highlight how the stator currents (id and iq), influenced by the stator resistance (Rs) and the permanent magnet flux (ψd and ψq), along with the rotor speed (ωr), determine the electromagnetic torque (Te) generated by the PMSM. By manipulating the stator currents through SVPWM control, the RMOC can regulate the motor's speed and torque output, propelling the electric vehicle. In essence, the RMOC leverages the existing SVPWM control strategy to effectively manage the PMSM in driving mode. This allows the converter to seamlessly switch between charging and driving functionalities, utilizing the same motor hardware for both operations.

3. Control Strategies for the RMOC: Charging and Driving Modes

The RMOC operates in distinct charging and driving modes, each requiring a dedicated control strategy. These strategies function independently as the modes cannot occur simultaneously.

A. Charging Mode Control with Interleaving

The primary objectives of the charging mode control strategy are:

- ***Unity Power Factor:*** This ensures efficient energy transfer from the AC grid to the battery, minimizing power loss.
- ***Reducing Current Ripple:*** Minimizing current fluctuations entering the battery promotes battery health and lifespan.
- ***Regulating Battery Charging:*** The control strategy precisely regulates either the charging voltage or current delivered to the battery.
- ***Interleaving Control for Ripple Reduction:*** To effectively address current ripple in the charging mode, the RMOC utilizes the interleaving control method. This method essentially splits the converter into two virtual "phases" driven with a 180-degree phase shift. The

Vol. 21, No. 1, (2024)
ISSN: 1005-0930

resulting input current represents the combined current from both virtual phases (inductors Lb and Lc).

- ***Mathematical Analysis of Ripple Reduction:***

Through mathematical equations (refer to equations 11-15), the control strategy analyses the impact of interleaving on current ripple:

$$I_{in} = \frac{V_B^2}{V_{in} R_L} = \frac{V_{in}}{(1-D)^2 R_L} \quad (11)$$

$$|\Delta_{im}| = \begin{cases} \frac{D(1-2D)}{1-D} \frac{(V_{in})}{3L_s f_s} \ (0 < D < 0.5) \\ (2D-1) \frac{V_m}{3L_s f_s} (0.5 < D < 1) \end{cases}$$

(12)

$$\delta = \begin{cases} \frac{D(1-2D)(1-D)V_{in}R_L}{3L_s f_s} (0 < D < 0.5) \\ \frac{(2D-1)(1-D)^2 R_L V_{in}}{3L_s f_s} (0.5 < D < 1) \end{cases}$$

(13)

$$|\Delta_{b,c}| = \begin{cases} \frac{D(D-2)}{1-D} \frac{(V_{in})}{3L_s f_s} \ (0 < D < 0.5) \\ (1+D) \frac{V_{in}}{3L_s f_s} (0.5 < D < 1) \end{cases}$$

(14)

$$\gamma(D) = \frac{|\Delta i_a|}{|\Delta i_{b,c}|} = \begin{cases} \frac{(1-2D)}{(2-D)} (0 < D < 0.5) \\ \frac{2D-1}{2-D} (0.5 < D < 1) \end{cases}$$

(15)

Equation (11) establishes the relationship between the input current (I_{in}), battery voltage (V_B), input voltage (Vin), load resistance (R_L), and duty cycle (D). Equation (12) quantifies the current ripple (Δim) with respect to switching frequency (fs), duty cycle (D), input voltage (Vin), and inductor inductance (L_s). This equation considers the duty cycle range ($0 < D < 0.5$ and $0.5 < D < 1$) to account for different operating conditions. Equation (13) expresses the ratio of current ripple to current amplitude (δ) as a function of duty cycle, input voltage, load resistance, switching frequency, and inductor inductance. This ratio provides a normalized metric for ripple reduction effectiveness. Equations (14) highlight that the current ripple amplitudes for both inductors (Ib and Ic) are identical but out of phase. These equations depict the ripple amplitude variation based on the duty cycle range. Finally, equation (15) introduces the concept of normalized current ripple (γ(D)). This metric compares the ripple in the proposed converter's single input current (|Δia|) to the ripple in each individual inductor current ($\Delta i_{b,c}$) for the traditional interleaved converter. The equation considers the duty cycle range for analysis.

Vol. 21, No. 1, (2024)
ISSN: 1005-0930

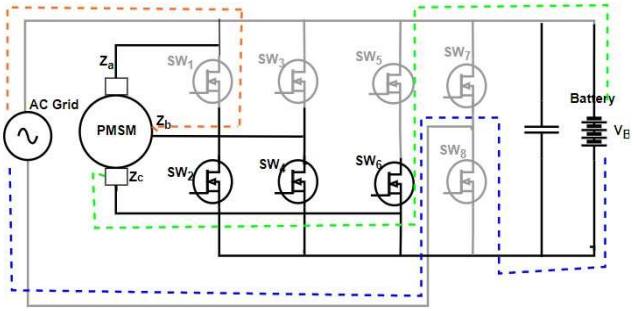

(a) Switching State Mode -I

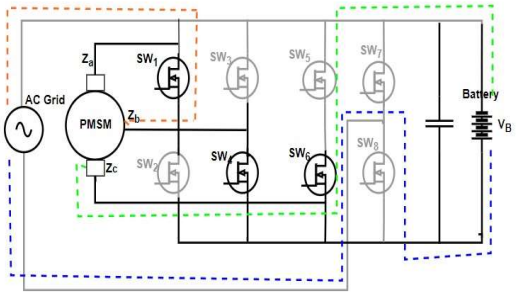

(b) Switching State Mode -II

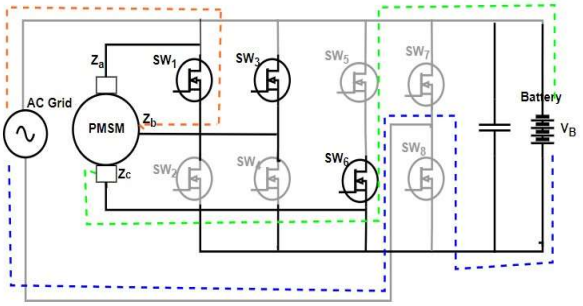

(c) Switching State Mode –III

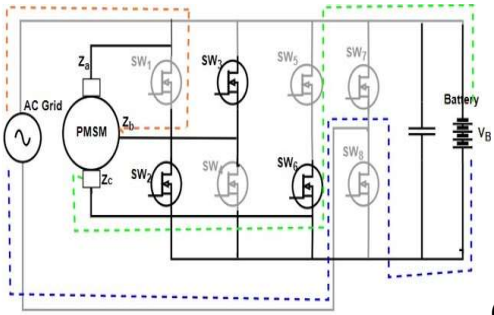

(d)

Switching State Mode -IV

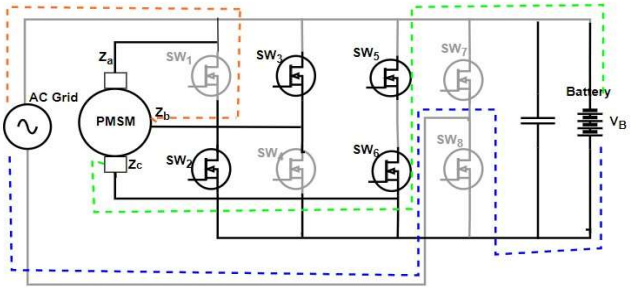

(e) Switching State Mode -V

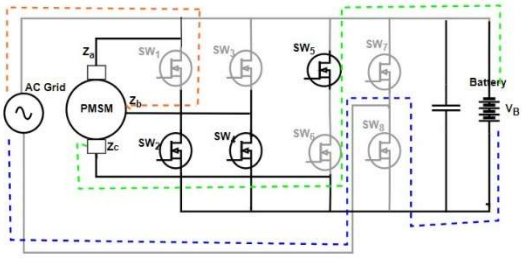

(f) Switching State Mode -VI

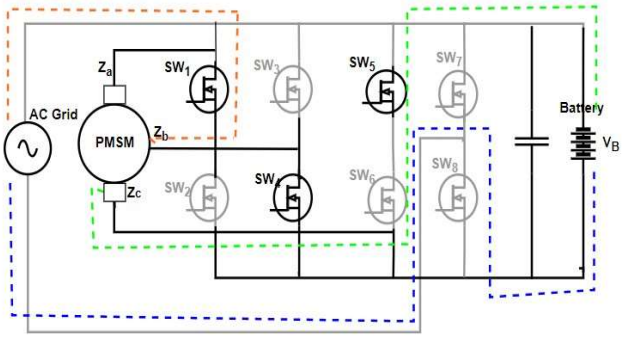

(g) Switching State Mode -VII

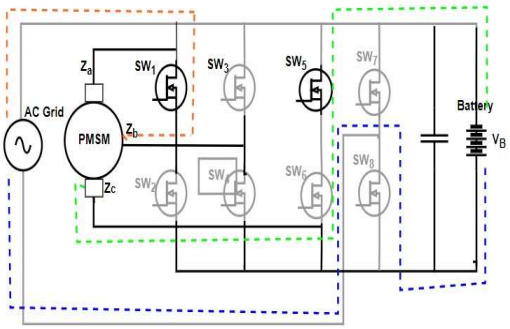

(h) Switching State Mode -VIII

Figure 5. The suggested RMOC exhibits varying states throughout the driving mode.

B. Ripple Reduction Effectiveness:

The effectiveness of ripple cancellation in both the conventional interleaved converter and the RMOC

that has been developed is depicted graphically in, which provides no further information. In the analysis, several important points are revealed: At a duty cycle of 0.5, the currently proposed RMOC is able to entirely eliminate current ripple, which is a benefit that is inherited from the conventional converter. When the duty cycle is lower than 0.5, the converter that has been proposed demonstrates a significant beneficial effect. When compared to the typical converter, the RMOC provides a current ripple that is only half as large. When compared to the conventional design, the RMOC continues to maintain a smaller current ripple even when faced with duty cycles that are more than 0.5.

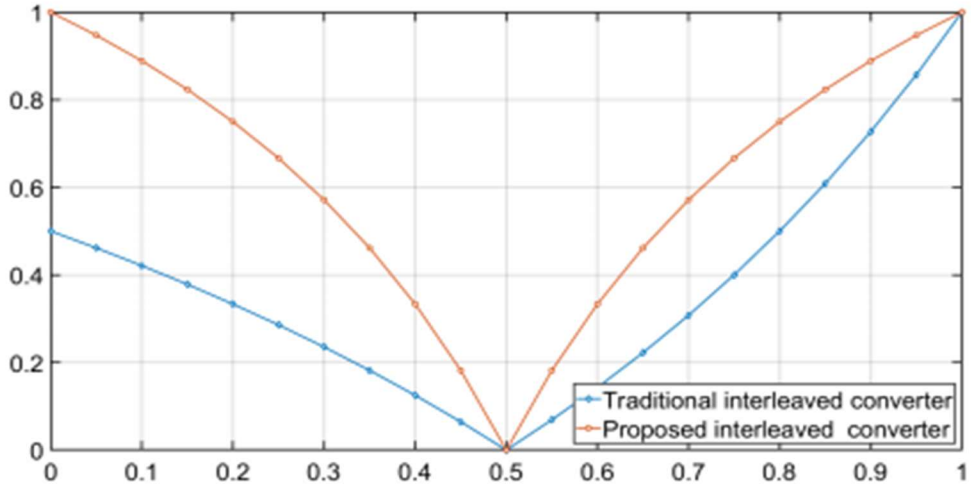

Figure 6. Ripple reduction effectiveness conventional switching state Mode converter and suggested converter

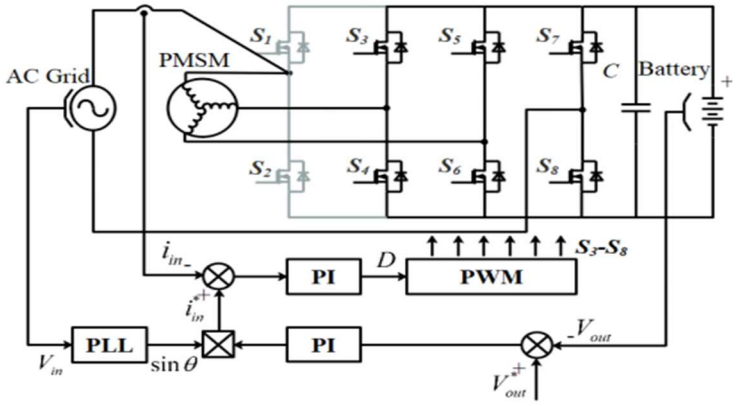

Figure 7. Control Structure for Charging Mode

In essence, the interleaving control strategy implemented in the proposed RMOC demonstrates superior effectiveness in reducing current ripple compared to the traditional approach. This translates to a cleaner and more efficient charging process for the electric vehicle's battery.

3.1 Unity Power Factor and Battery Charging Regulation Control Strategy

The charging mode control strategy in the RMOC addresses two critical objectives:

1. Achieving Unity Power Factor: This ensures that the current drawn from the AC grid is in phase

with the grid voltage, minimizing reactive power loss and maximizing energy transfer efficiency.

2. Regulating Battery Charging Voltage: The control strategy precisely regulates the voltage delivered to the battery, ensuring a safe and controlled charging process. Dual Closed-Loop Control System (refer to Figure 5):

The proposed control strategy utilizes a dual closed-loop system for effective regulation:

- ***Inner Current Loop:*** This loop focuses on achieving unity power factor. It employs a phase-locked loop (PLL) to synchronize the phase of the input current with the grid voltage. This ensures that the current waveform aligns perfectly with the voltage waveform, minimizing reactive power and achieving a power factor of one.
- ***Outer Voltage Loop:*** The outer loop manages the overall charging process. It adjusts the amplitude of the input current based on the desired charging voltage for the battery. By manipulating this current amplitude, the control system regulates the voltage delivered to the battery.

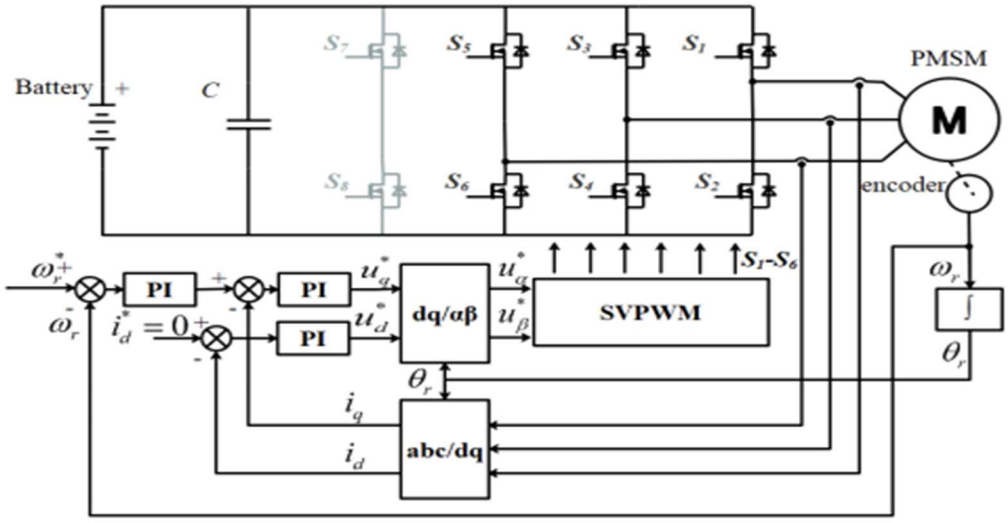

Figure 8. Driving-mode RMOC control block.

Operational Details Based on Grid Voltage Polarity:

Positive Grid Voltage: When the grid voltage is positive, switch S7 remains off, and S8 is turned on. Switches S4 and S6 are controlled by independent drive signals with a 180-degree phase shift, implementing the interleaving control strategy discussed earlier. Additionally, switches S3 and S5 function in a synchronous rectification mode, further enhancing efficiency.

Negative Grid Voltage: During negative grid voltage conditions, the operational behavior mirrors the positive voltage scenario. The switching patterns and control principles remain consistent, ensuring seamless operation regardless of grid voltage polarity.

In essence, the proposed control strategy leverages a combination of inner current loop (PLL) and outer voltage loop control to achieve two key goals: maximizing power transfer efficiency by achieving unity power factor and precisely regulating the charging voltage delivered to the battery.

Vol. 21, No. 1, (2024)
ISSN: 1005-0930

3.2. Control Strategy for Motor Vehicles Operating in Driving Mode

When the RMOC transitions to driving mode, the focus shifts to controlling the Permanent Magnet Synchronous Motor (PMSM) for optimal vehicle propulsion. Here's how the control strategy accomplishes this:

- **Switch Activation and Control:** Switches S1-S6 are activated in this mode. These switches are controlled using the Sinusoidal Pulse Width Modulation (SVPWM) technique (refer to FIGURE 6 for the control block diagram). SVPWM strategically generates switching patterns for the inverter, effectively creating the desired voltage waveforms that control the motor's speed and torque output.
- **Reference Current Generation:** The q-axis reference current for the stator current is derived from the speed closed-loop control system. This ensures that the motor's speed aligns with the desired vehicle speed.
- **d-axis Current Regulation:** The d-axis reference current for the stator is maintained at zero. This simplifies the control strategy and optimizes motor performance.

For a more in-depth exploration of the vector control method employed for PMSMs, you can refer to the resources mentioned in [23]. In summary, the driving mode control strategy utilizes SVPWM to control the PMSM based on reference currents derived from the speed control loop. This allows for precise regulation of the motor's speed, enabling efficient propulsion of the electric vehicle.

4. Simulation Results: Input Current Quality and Harmonic Distortion

A better understanding of the efficiency of the **Reconfigured Multi-Functional On-board Converter** (RMOC) concept that was proposed is provided by the results of the simulation.

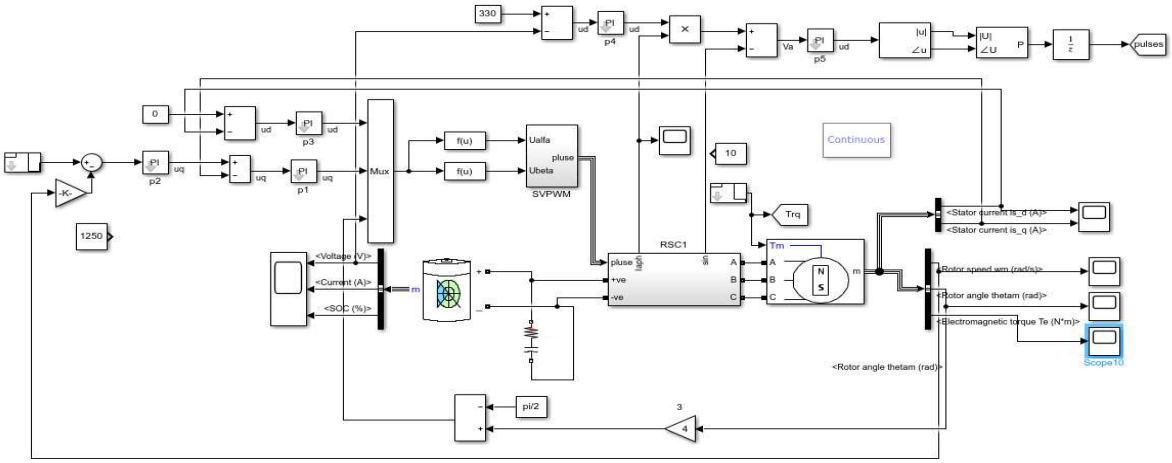

Figure 9. The MATLAB/ Simulink diagram of the PMSMS Electric Vehicle system with 8 switches under Driving and Charging modes

The simulation model of the total electric vehicle system is shown in Figure 9. There are eight switches in the circuit, with first 6 switches S1 to S6 operates with 1 phase AC supply with the proposed circuit and will drive the motor. The Switches S3 to S8 will be used to charge the battery under braking mode. The driving and charging mode circuits are shown in Figure 6 and 7. The

Vol. 21, No. 1, (2024)
ISSN: 1005-0930

existing designs typically exhibit higher current ripple ratios (ranging from 2.6% to 12.9%) and comparable or slightly better THD (between 3.96% and 6.15%). The proposed RMOC effectively suppresses input current ripple, resulting in a cleaner current waveform for the AC grid. The implemented control strategy significantly reduces THD compared to existing designs, signifying a more efficient energy transfer process. Interestingly, the proposed design achieves current ripple performance comparable to a scheme using a specialized motor (reference [19]). However, the RMOC offers a simpler system structure by eliminating the need for such a motor. Overall, the simulation results convincingly demonstrate the effectiveness of the proposed RMOC design. The combination of low current ripple and minimal THD translates to efficient and clean energy transfer from the AC grid to the battery, making it a promising solution for electric vehicle charging applications. The simulation results presented in Figure 9 assess the quality of the input current drawn by the RMOC and the (amount) of harmonic distortion (THD) introduced into the AC grid.

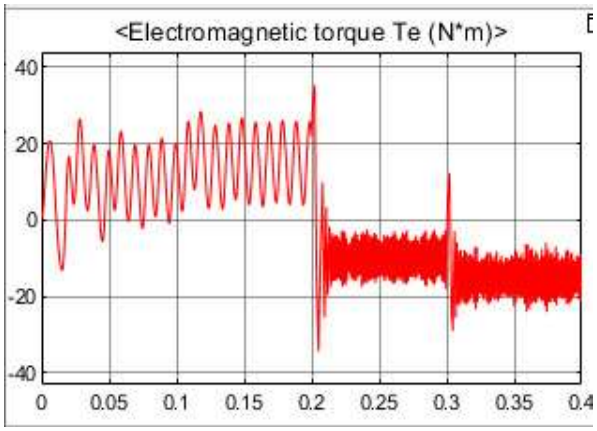

(a) Electromagnetic Torque (Nm) of PMSM

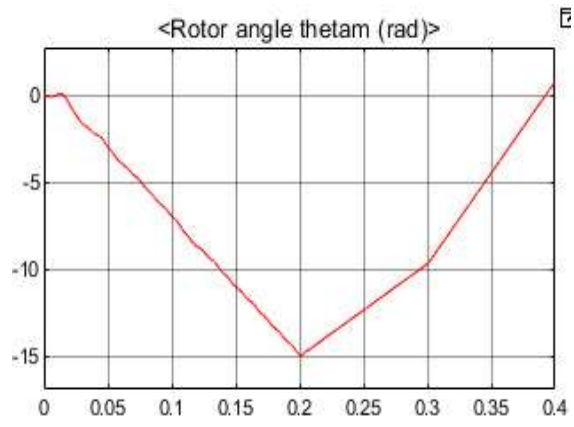

(b) Rotor angle (rad)

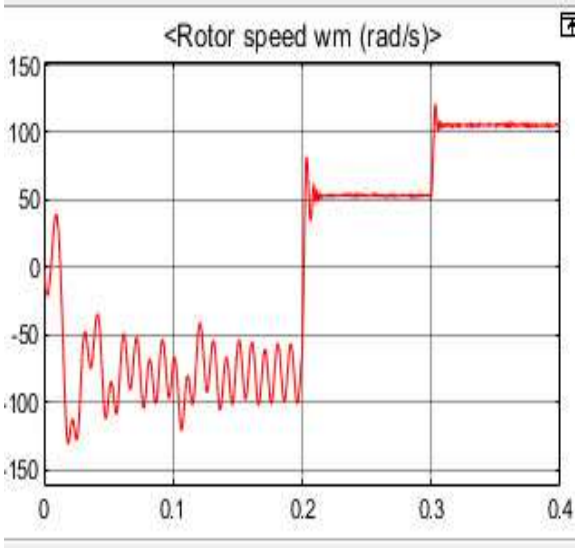

(c) Rotor speed (rad/sec)

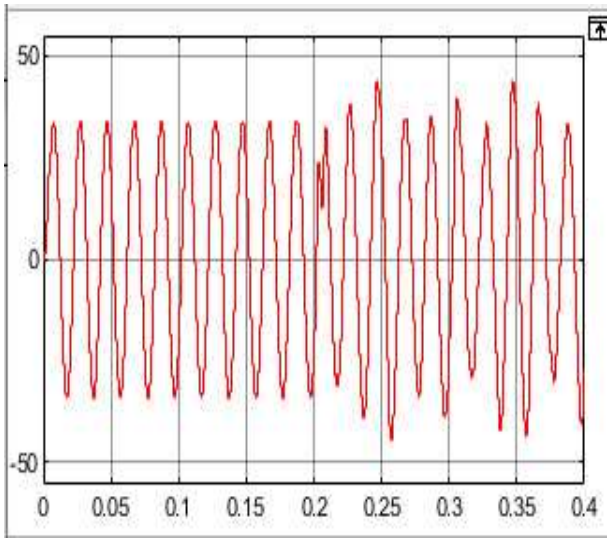

(d) Stator current (A-phase)

Vol. 21, No. 1, (2024)
ISSN: 1005-0930

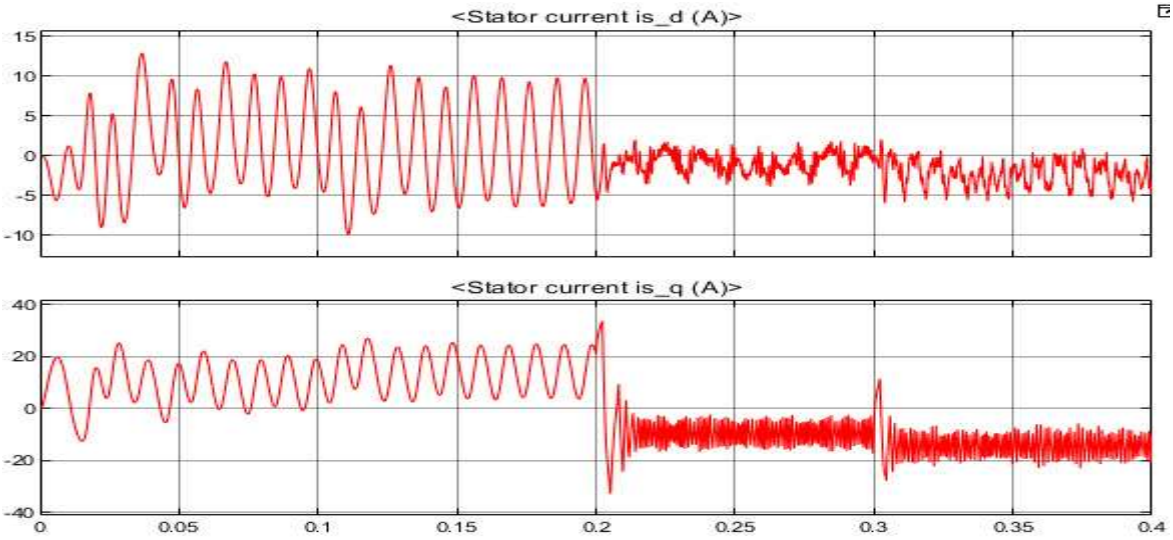

(e) d and q axis stator current of the PMSM electric drive system

Figure 10 .PMSM electric vehile parameters values under Charging (0 to 0.2 seconds) and Driving mode (0.2 to 0.44s).

The electric vehicle PMSM torque from to 0.1s is 10 Nm, 0.1 to 0.2s its variations is 15 Nm, 0.2 to 0.3s the torque changes to -10Nm and finally the torque varied to -15Nm at 0.4s as in Figure 10(a), the rotor angle changes with respect to these torque variations as in Fig. 10(b). It can be observed that the torque variations are positive implies the motor is in braking mode and the rotor angle is decreasing, while the torque which is negative from 0.2s, the motor is in driving mode and the rotor angle is increasing in amplidue and angle with increase in the torque value. With these changes the rotor speed is also changing as in Fig. 10(c) and can be observed that the speed directions are also reversing with the torque polarity from from positive to negative at 0.2s. The A-phase current of the PMSM is shown in Fig. 10(d) and it can be observed that the current is very sinusoidal without harmonics and the current angle also changed at 0.2s. In the same way the d and q-axis currents are changing with the change in the torque. In this, the d-axis current is almost zero as intended and the q-axis current is varying with increase in the load (torque) value as in Fig. 10(e). It can further be observed that the d and q axis currents are oscillatory during braking mode which is a natural phenomenon, while in driving mode the characteristics are linear.

Table 1. Comparative of **Reconfigured Multi-Functional On-board Converter** - (RMOC)

(RMOC) suggested approach	Ref[14]	Ref [19]	Ref [21]	Ref [27]	Ref [28]	suggested approach
Customised Motor	Yes	Yes	NO	NO	Yes	NO
Auxiliary equipment	No	Yes	Yes	Yes	No	No

Vol. 21, No. 1, (2024)
ISSN: 1005-0930

The quantity of power switches	12	6	12	6	12	8
THD	Middle	Low	High	Low	Low	Low
Size	Low	Middle	Low	Middle	High	Low
Cost	High	High	Low	Middle	High	Low

Key Observations:

- The proposed RMOC demonstrates superior performance in suppressing input current ripple, resulting in a cleaner current waveform fed back to the AC grid.
- Compared to [18] and [21], the proposed control strategy significantly reduces the THD, indicating a more sinusoidal and efficient current waveform.
- Interestingly, the proposed RMOC achieves an input current ripple comparable to the scheme using a specially designed motor in [19]. However, the proposed design offers a simpler system structure by eliminating the need for such a motor.

In essence, the simulation results validate the effectiveness of the proposed control strategy in achieving a clean and low-distortion input current for the RMOC. This translates to efficient energy transfer from the AC grid to the battery while minimizing harmonic distortion.

5. Conclusion

This paper presented a novel Reconfigured Multi-Functional On-board Converter (RMOC) designed specifically for Plug-in Electric Vehicles (PEVs). The proposed RMOC offers several key advantages over existing solutions. Unlike existing designs that may require specially designed motors or additional AC-side equipment, the RMOC leverages a simple modification to the existing three-phase motor drive converter. This modification involves adding a set of auxiliary switches in the DC side. This streamlined approach translates to a more compact and cost-effective solution. The RMOC seamlessly integrates with existing charging infrastructure, allowing connection to a standard power outlet without needing extra power supply equipment. The implemented interleaving control strategy effectively reduces the current ripple in the charging mode. This not only improves battery health but also minimizes harmonic distortion fed back to the AC grid, ensuring efficient and clean energy transfer. Simulation results convincingly demonstrate the RMOC's effectiveness in achieving low input current ripple and minimal THD, surpassing the performance of traditional converters. Furthermore, successful workbench verification confirms the RMOC's ability to fulfil both motor drive and battery charging functions, making it a versatile solution for PEV applications. In summary, the proposed RMOC presents a compelling alternative for PEV onboard charging. Its combination of simplicity, cost-effectiveness, efficient power transfer, and verified functionality positions it as a promising technology for advancing the future of electric mobility.

References

[1] Chan, A. Bouscayrol, and K. Chen, ‘‘Electric, hybrid, and fuel-cell vehicles: Architectures and modeling,’’ *IEEE Trans. Veh. Technol*., vol. 59, no. 2, pp. 589–598, Feb. 2010.

[2] S. Kumar and A. Usman, ‘‘A review of converter topologies for battery charging applications in plug-in hybrid electric vehicles,’’ in Proc. *IEEE Ind. Appl. Soc. Annu. Meeting (IAS),* Portland, OR, USA, Sep. 2018, pp. 1–9.

[3] Berthold, A Ravey, B. Blunier, D. Bouquain, S. Williamson, and A. Miraoui, ‘‘Design and development of a smart control strategy for plugin hybrid vehicles including vehicle-to-home functionality,’’ *IEEE Trans. Transport. Electrics*., vol. 1, no. 2, pp. 168–177, Aug. 2015.

[4] Rezaei, J. B. Burl, M. Rezaei, and B. Zhou, ‘‘Catch energy saving opportunity in charge-depletion mode, a real-time controller for plugin hybrid electric vehicles,’’ *IEEE Trans. Veh. Technol*., vol. 67, no. 11, pp. 11234–11237, Nov. 2018.

[5] F. Ahmadi, E. Adib, and M. Azari, ‘‘Soft switching bidirectional converter for reflex charger with minimum switches,’’ *IEEE Trans. Ind. Electron.,* to be published.

[6] U. Yilmaz, O. Turksoy, and A. Teke, ‘‘Intelligent control of high energy efficient two-stage battery charger topology for electric vehicles,’’ *Energy*, vol. 186, Nov. 2019, Art. no. 115825.

[7] F. Yu, W. Zhang, Y. Shen, and J. Mao, ‘‘A nine-phase permanent magnet electric-drive-reconstructed onboard charger for electric vehicle,’’ *IEEE Trans. Energy Convers*., vol. 33, no. 4, pp. 2091–2101, Dec. 2018.

[8] M. Yilmaz and P. T. Krein, ‘‘Review of battery charger topologies, charging power levels, and infrastructure for plug-in electric and hybrid vehicles,’’ *IEEE Trans. Power Electron*., vol. 28, no. 5, pp. 2151–2169, May 2013.

[9] S. Haghbin, K. Khan, S. Landmark, M. Alakla, O. Carlson, M. Leksell, and O. Wall mark, ‘‘Integrated chargers for EV’s and PHEV’s: Examples and new solutions,’’ *in Proc. 19th Int. Conf. Elect. Mach.-ICEM,* Sep. 2010, pp. 1–6.

[10] M. Grenier, T. Thiringer, and M. Aghdam, ‘‘Design of on-board charger for plug-in hybrid electric vehicle,’’ *in Proc. 5th IET Int. Conf. Power Electron., Mach. Drives (PEMD),* 2010, pp. 1–6.

[11] S. Morimoto, S. Ooi, Y. Inoue, and M. Sanada, ‘‘Experimental evaluation of a Rare-Earth-free PMASynRM with ferrite magnets for automotive applications,’’ *IEEE Trans. Ind. Electron.,* vol. 61, no. 10, pp. 5749–5756, Oct. 2014.

[12] J. Nerg, M. Rilla, V. Ruuskanen, J. Pyrhonen, and S. Ruotsalainen, ‘‘Direct-driven interior magnet permanent-magnet synchronous motors for a full electric sports car,’’ *IEEE Trans. Ind. Electron.*, vol. 61, no. 8, pp. 4286–4294, Aug. 2014.

[13] Y. Tang, W. Ding, and A. Khaligh, ‘‘A bridgeless totem-pole interleaved PFC converter for plug-in electric vehicles,’’ in Proc. *IEEE Appl. Power Electron. Conf. Expo. (APEC),* Mar. 2016, pp. 440–445.

[14] L. De Sousa, B. Silvestre, and B. Bouchez, ‘‘A combined multiphase electric drive and fast battery charger for electric vehicles,’’ in Proc. IEEE Vehicle Power Propuls. Conf., Sep. 2010, pp. 1–6.

[15] A. Bruyère, L. De Sousa, B. Bouchez, P. Sandulescu, X. Kestelyn, and E. Semail, ‘‘A multiphase traction/fast-battery-charger drive for electric or plug-in hybrid vehicles: Solutions for control in traction mode,’’ in Proc. *IEEE VPPC*, Sep. 2010, pp. 1–7.

[16] S. Lacroix, E. Laboure, and M. Hilairet, ‘‘An integrated fast battery charger for electric vehicle,’’ in Proc. *IEEE Vehicle Power Propuls*. Conf., Sep. 2010, pp. 1–6.

[17] S. Haghbin, S. Lundmark, M. Alakula, and O. Carlson, ‘‘An isolated high power integrated charger in electrified-vehicle applications,’’ *IEEE Trans. Veh. Technol*., vol. 60, no. 9, pp. 4115–4126, Nov. 2011.

[18] S. Haghbin, S. Lundmark, M. Alakula, and O. Carlson, ‘‘Grid-connected integrated battery chargers in vehicle applications: Review and new solution,’’ *IEEE Trans. Ind. Electron*., vol. 60, no. 2, pp. 459–473, Feb. 2013.

[19] L. Solero, ‘‘Nonconventional on-board charger for electric vehicle propulsion batteries,’’ IEEE Trans. Veh. Technol., vol. 50, no. 1, pp. 144–149, Jan. 2001.

[20] L. Tang and G.-J. Su, ‘‘A low-cost, digitally-controlled charger for plugin hybrid electric vehicles,’’ in Proc. *IEEE Energy Convers. Congr. Expo*., Sep. 2009, pp. 3923–3929.

[21] J. Ye, C. Shi, and A. Khaligh, ‘‘Single-phase charging operation of a three phase integrated onboard charger for electric vehicles,’’ in Proc. *IEEE Transp. Electrific. Conf. Expo (ITEC),* Long Beach, CA, USA, Jun. 2018, pp. 681–686.

[22] C. Shi, Y. Tang, and A. Khaligh, ‘‘A three-phase integrated onboard charger for plug-in electric vehicles,’’ *IEEE Trans. Power Electron*., vol. 33, no. 6, pp. 4716–4725, Jun. 2018.

[23] J. Wu, J. Wang, C. Gan, Q. Sun, and W. Kong, ‘‘Efficiency optimization of PMSM drives using field-circuit coupled FEM for EV/HEV applications,’’ *IEEE Access*, vol. 6, pp. 15192–15201, 2018.

[24] C. Yunyun, Q. Li, Z. Xiaoyong, W. Hua, and Z. Wang, ‘‘Electromagnetic performance analysis of double-rotor stator permanent magnet motor for hybrid electric vehicle,’’ *IEEE Trans. Magn.,* vol. 48, no. 11, pp. 4204–4207, Nov. 2012.

[25] A. V. Sant, V. Khadkikar, W. Xiao, and H. H. Zeineldin, ‘‘Four-axis vector controlled dual-rotor PMSM for plug-in electric vehicles,’’ *IEEE Trans. Ind. Electron*., vol. 62, no. 5, pp. 3202–3212, May 2015.

[26] M. C. Kisacikoglu, M. Kesler, and L. M. Tolbert, ‘‘Single-phase on-board bidirectional PEV charger for V2G reactive power operation,’’ *IEEE Trans. Smart Grid*, vol. 6, no. 2, pp. 767–775, Mar. 2015.

[27] A. G. Cocconi, ‘‘Combined motor drive and battery recharge system,’’ *U.S. Patent* 5 341 075 A, Aug. 23, 1994.

[28] D.-G. Woo, G.-Y. Choe, J.-S. Kim, B.-K. Lee, J. Hur, and G.-B. Kang, ‘‘Comparison of integrated battery chargers for plug-in hybrid electric vehicles: Topology and control,’’ *in Proc. IEEE Int. Electr. Mach. Drives Conf. (IEMDC)*, Niagara Falls, ON, Canada, May 2011, pp. 1294–1299.

[29] G. Pellegrino, E. Armando, and P. Guglielmi, ‘‘An integral battery charger with power factor correction for electric scooter,’’ *IEEE Trans. Power Electron*., vol. 25, no. 3, pp. 751–759, Mar. 2010.

[30] S. Sun, Q. Yang, and W. Yan, ‘‘A novel Markov-based temporal-SoC analysis for characterizing PEV charging demand,’’ *IEEE Trans. Ind. Informat*., vol. 14, no. 1, pp. 156–166, Jan. 2018.

[31] N. Neyestani, M. Y. Damavandi, G. Chicco, and J. P. S. Catalao, ‘‘Effects of PEV traffic flows on the operation of parking lots and charging stations,*’’ IEEE Trans. Smart Grid*, vol. 9, no. 2, pp. 1521–1530, Mar. 2018.

[32] X. Sun, Z. Shi, G. Lei, Y. Guo, and J. Zhu, ‘‘Analysis and design optimization of a permanent magnet synchronous motor for a campus patrol electric vehicle,’’ *IEEE Trans*. Veh. Technol., vol. 68, no. 11, pp. 10535–10544, Nov. 2019.

[33] S. Haghbin, M. Alakula, K. Khan, S. Lundmark, M. Leksell, O. Wallmark, and O. Carlson, ‘‘An integrated charger for plug-in hybrid electric vehicles based on a special interior permanent magnet motor,’’ in Proc. *IEEE Vehicle Power Propuls. Conf.,* Sep. 2010, pp. 1–6.

[34]